Holographic image of a point source in the presence of misalignment

I. Banyasz, G. Kiss, and P. Varga

The imaging of a point source by high numerical aperture holograms was studied theoretically and experimentally in the presence of aberrations caused by inaccurate adjustment of the plane reference and plane reconstructing waves or by inaccurate positioning of the hologram. The accuracy requirement is defined by the angular resolution allowed by an aperture equal to the hologram size. Any deviation from this limit leads to deformation of the point transfer function defined by the unavoidable diffraction. For coarse mismatch ($>10^{-3}$ rad for the actual case), clearly demonstrable geometrical-type aberrations occur; for smaller angles, appreciable broadening of the diffraction pattern and rapid fall of the Strehl ratio diminish the applicability of the holographic method. The calculations and the photographic and photometric measurements are in good agreement.

I. Introduction

Holograms seem to be the best optical elements when high resolution and large object field area are simultaneously required, e.g., in holographic microscopy, bubble chamber holography, photolithography. The resolving power of holograms is mainly limited by the finite wavelength and aperture. When the primary diffraction limits are approached, further restrictions are set by the resolving capability of the recording material,[1] furthermore the shrinkage of the photolayer causes additional decrease of the diffraction efficiency at higher spatial frequencies.[2] Besides these limitations there are some practical obstacles preventing one from reaching the theoretical limits—mainly that the experimental conditions do not satisfy the demands under which the speculative predictions are valid.

With holographic microscopy the existence of aberrations is *ab ovo* obvious[3–6] because the auxiliary waves are spherical and have different curvature, consequently the reconstructed wavefront of a point object suffers the same defects as the wavefront at the exit of a spherical lens. In the case of holographic lithography, plane auxiliary waves are preferred. Any angular mismatch between the auxiliary waves or inaccurate reposition of the hologram plate after development leads to deformation of the reconstructed wavefront. The aim of this paper is to study quantitatively the influence of the mismatch on the point spread function both theoretically and experimentally. For large mismatch angles (more than a minute of arc), photographic recording of the image pattern seemed to be satisfactory; for small angles, instead of the usual visual observation we preferred to measure the intensity distribution.

II. Geometrical-Type Aberrations

The model investigated is shown in Fig. 1. A point source in $P_o(x_o,y_o,z_o)$ gives rise to a spherical wave and is recorded in the hologram plane $z = 0$. The reference wave is a plane one with wave vector $\mathbf{k}_r = k(\cos\kappa_r, \cos\mu_r, \cos\nu_r)$. For the reconstruction another plane wave is used having the wave vector $\mathbf{k}_c = k(\cos\kappa_c, \cos\mu_c, \cos\nu_c)$. If the auxiliary waves are exactly opposite in direction and have the same wavelength, the reconstructed wavefront emerging from the hologram is the complex conjugate of the object wave and focuses itself at the original object point P_o. If the auxiliary waves are mismatched, ray aberrations take place around some point $P_i(x_i,y_i,z_i)$ which may be regarded to be the image of the object at P_o.

According to Ref. 3 the aberration of the wavefront (Δ) is the sum of the phases of all four waves taking part in the reconstruction.

$$k\Delta = kr_i - kr_o - (\mathbf{k}_r + \mathbf{k}_c)\mathbf{r}, \tag{1}$$

where r_o and r_i are the object and the image distances from any point of the hologram, respectively.[8] On

The authors are with Central Research Institute for Physics, P.O. Box 49, Budapest 1525, Hungary.

Received 26 June 1987.
0003-6935/88/071293-05$02.00/0.

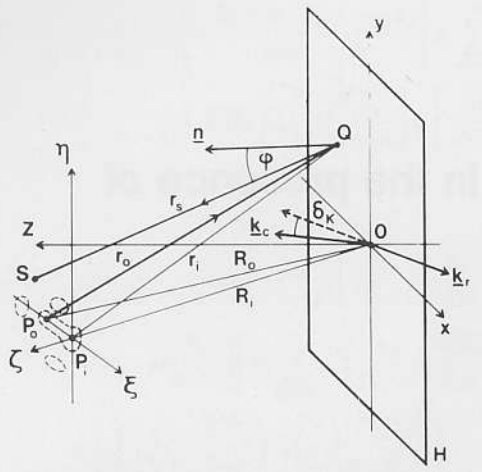

Fig. 1. Schematic diagram of hologram recording and reconstruction.

introducing a local coordinate frame ξ,η,ζ fixed to the image P_i as the origin, the ray emerging from a hologram point $Q(x,y)$ goes through the point $S(\xi,\eta,\zeta)$ defined by

$$\xi = -\frac{\zeta x}{R_o} + R_o \frac{\partial \Delta}{\partial x}, \qquad \eta = -\frac{\zeta y}{R_o} + R_o \frac{\partial \Delta}{\partial y} \tag{2}$$

(see Ref. 7).

For small angular mismatch $(\delta_\kappa,\delta_\mu)$ of the auxiliary waves, the plane wave term in Eq. (1) can be expressed as (say)

$$\begin{aligned} \cos\kappa_r + \cos\kappa_c &= -\sin\kappa_r \cdot \delta_\kappa = \alpha, \\ \cos\mu_r + \cos\mu_c &= -\sin\mu_r \cdot \delta_\mu = \beta. \end{aligned} \tag{3}$$

We make an expansion of the distance r_q $(q = o,i)$ into a series up to the third term:

$$r_q = R_q \left\{ 1 + \frac{x^2 + y^2 - 2(xx_q + yy_q)}{2R_q^2} + \frac{[x^2 + y^2 - 2(xx_q + yy_q)]^2}{8R_q^4} \right\}, \tag{4}$$

where R_q is the distance of $P_Q(x_q,y_q,z_q)$ from the hologram center. Substituting the zero- and first-order terms into Eq. (1) the coefficients of x and y will identically be zero if

$$R_i = R_o, \tag{5}$$

$$x_i = x_o + \alpha R_o, \qquad y_i = y_o + \beta R_o, \tag{6}$$

i.e., the image is reconstructed at the same distance from the hologram center but shifted as a consequence of the mismatch. (For a tilted hologram the coordinate frame is to be fixed to the hologram itself.) Inserting the fourth-order terms into Eq. (1) and taking into account Eqs. (3) and (4), for the perturbation of the wavefront we obtain

$$\Delta = \frac{\alpha x + \beta y}{R_0^2} \left[\frac{1}{2}(x^2 + y^2) - (xx_o + yy_o) \right] \tag{7}$$

(second-order terms of α and β have been neglected). Using Eqs. (2) for the ray aberration we obtain

$$\begin{aligned} \xi &= R_0^{-1} \{ -\zeta x - [2\alpha x x_o + (\alpha y_o + \beta x_o) y] + \tfrac{1}{2}(3\alpha x^2 + 2\beta xy + \alpha y^2) \}, \\ \eta &= R_o^{-1} \{ -\zeta y - [2\beta y y_o + (\alpha y_o + \beta x_o) x] + \tfrac{1}{2}(\beta x^2 + 2\alpha xy + 3\beta y^2) \}. \end{aligned} \tag{8}$$

The term in brackets corresponds to the astigmatism and the term in parentheses corresponds to the coma. Astigmatism occurs for the off-axis points only, the coma is independent of the location of the object. If the size of an extended object is less than that of the hologram, coma plays a major role. Note that no spherical aberration occurs.

If the numerical aperture of the holographic recording system is 0.5, the diameter of the hologram is 60 mm and the mismatch is 1 mrad, then the light is spread out in a region of 30-μm diameter which is larger than that of any expectable diffraction pattern.

We carried out experiments to verify Eq. (8) in the simplest way so the object was inclined in the $y = 0$ plane. Instead of changing the direction of the reconstructing beam the hologram was rotated around the y axis, in this way the sole variable parameter was the angular rotation. Thus Eq. (8) becomes

$$\begin{aligned} \xi &= \frac{\rho}{R_o} \left[-(\zeta + 2\alpha x_o)\cos\vartheta + \alpha\rho \left(1 + \frac{1}{2}\cos 2\vartheta \right) \right], \\ \eta &= \frac{\rho}{R_o} \left[-\zeta \sin\vartheta + \frac{1}{2}\alpha\rho \sin 2\vartheta \right], \end{aligned} \tag{9}$$

where ρ and ϑ are the polar coordinates in the hologram plane.

In the experimental setup the point light source P_o (see Fig. 1) was formed from a He–Ne laser beam with a lens of 0.85 N.A. To verify the calculations and to demonstrate the character of the pattern suffering from aberration we illuminated the hologram by a plane wave through a ring aperture positioned in front of the hologram. The diameters of the rings were 10, 15, 20, and 25 mm, their width was 10 mm. The reconstructed pattern was photographed in three planes: in the meriodional image plane ($\zeta = 0$), in the sagittal plane ($\zeta = 2\alpha x$), and in the plane on the midway. The diameters of the rings were 10, 15, 20, and 25 mm, their width was 10 mm. The meridional plane coincides with the object plane, the latter was fixed by the focus of the objective producing the object source. The separations of the two other planes were measured relative to this plane. In the experiments we took good care to approximate the conditions to the theoretical ones. Auxiliary waves were produced by large aperture telescopes to cover the hologram with nearly uniform illumination, in each case the flatness of the wavefront was thoroughly checked by shearing interference.

In Figs. 2–4 demonstrate the aberration curves in the three planes mentioned. Calculations and measurements were carried out for the source distance $R_o = 90$ mm, its position was at $x_o = R_o \sin 22.5°$ and the angle of incidence of the reference beam was $\kappa_r = 22.5°$.

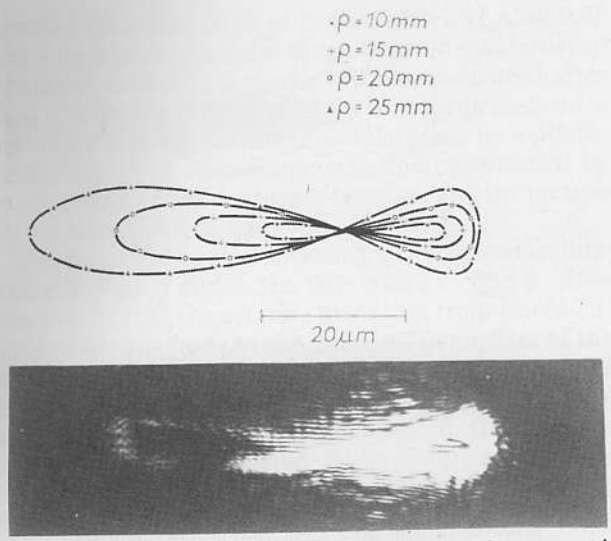

Fig. 2. Pattern reconstructed from a ring forming hologram part in the meridional plane for a misalignment of 6 mrad. Calculated curves (above) for hologram mean radii ρ = 10, 15, 20, and 25 mm; photographed pattern (below) for mean radius = 20 mm.

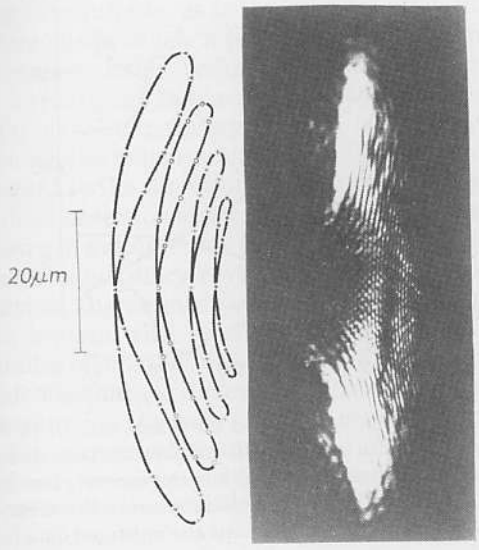

Fig. 3. Pattern in the sagittal plane; the other data as in Fig. 2.

Dots on the continuous curves correspond to equidistant points on the ring aperture so we can also estimate the intensity distribution. In the lower part of each figure the photographed pattern is demonstrated for the ring's mean radius of 20 mm. For more qualitative evaluation we measured some characteristic parameters of the patterns. Figure 5 shows the measured values of two typical parameters of the eight forming patterns in the meridional plane and the expected mean length of this pattern. For other parameters a similar coincidence was obtained between calculated and observed data.

III. Aberrations Combined with Diffraction

For small angles the broadening of the image pattern due to inaccuracy is commensurable with the diffraction broadening. Instead of the Hartmann type figures we took advantage of microphotometry and compared the results to the calculated distribution.

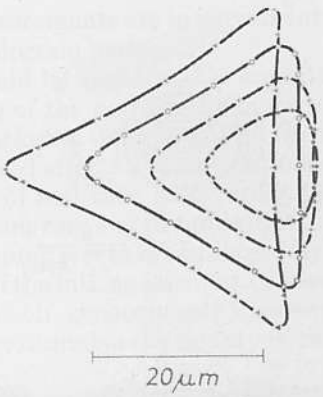

Fig. 4. Pattern in the plane of less confusion; the other data as in Fig. 2.

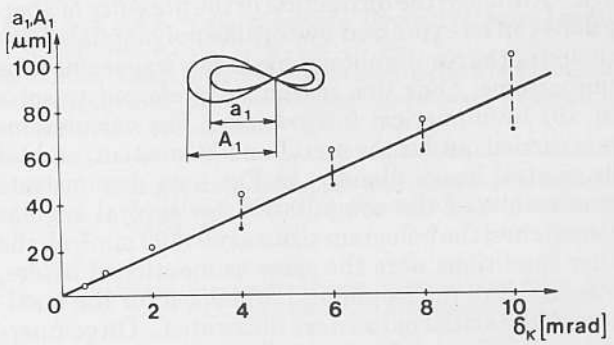

Fig. 5. Measured dimensions of the internal and external loops of the meridional pattern and the calculated medial dimension vs the mismatch angle.

In the case of mismatch between the auxiliary beams the reconstructed field can be expressed by the Fresnel-Kirchhoff integral

$$u(\xi,\eta,\zeta) = \iint_H \frac{\cos\varphi}{r_s r_o} \exp[ik(r_s - r_o + x \sin\kappa_r \cdot \delta_\kappa)]dxdy, \quad (10)$$

where φ is the inclination angle; for the other notations see Fig. 1; the integral is to be taken over the hologram

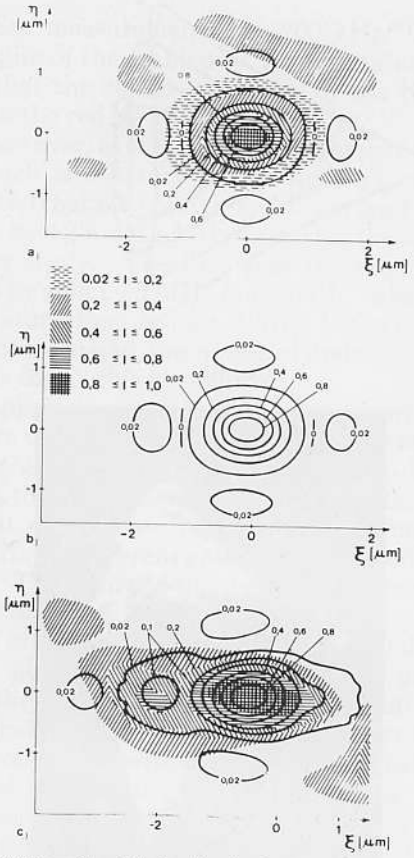

Fig. 6. Light intensity distribution in the meridional plane for (a) ideal adjustment, and for mismatch angles (b) 10^{-5} rad and (c) 5×10^{-5} rad. The calculated isophotes are continuous lines; the measured data are illustrated by shading (see insert)

area. Although the diffraction in the presence of aberrations can be expressed by Zernike polynomials,[9] discussion of the results obtainable in this way seems to be cumbersome. For this reason we preferred to solve Eq. (9) by numerical integration. The calculations were carried out for the meridional (Gaussian) and for the sagittal image planes. In Fig. 6 we demonstrate some results of the computation for several angular mismatches; the hologram size was 60×90 mm^2; all the other conditions were the same as mentioned before. In each figure the isophotes normalized for the maximum of the actual pattern are illustrated. On comparing the distribution for the ideal case with the same for $\delta_\kappa = 10^{-5}$ rad, we found no difference except the shift of the patterns. The identity of the two patterns is obvious because the angular resolution of the whole hologram plate is the same.

When the mismatch is $\delta_\kappa = 5 \times 10^{-5}$ rad (10 sec of arc) a noticeable change in the low intensity part of the distribution can be observed. The central part of the pattern ($I > 40\%$) remains nearly unchanged but the low intensity wings become wider. Consequently, if an object consisting of parallel bars is to be recorded the spurious interference of their wings may cause ghosts.[10] It seems that the conditions for diminishing coma and astigmatism (11 and 7 sec of arc, respectively) published in Ref. 4 were underestimated.

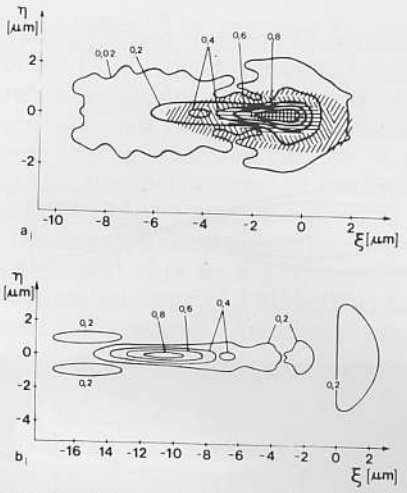

Fig. 7. Light intensity distribution in the meridional plane for mismatch angles (a) 2×10^{-4} rad and (b) 10^{-3} rad.

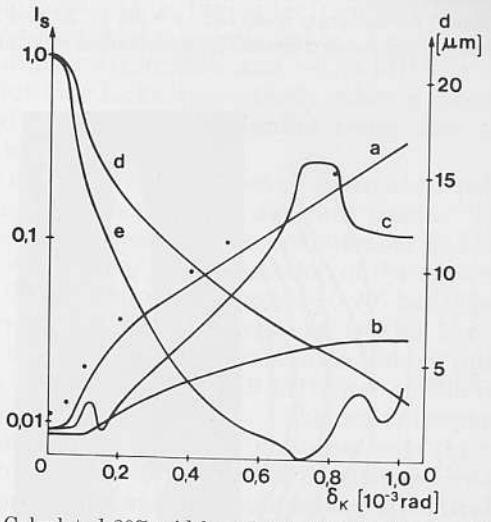

Fig. 8. Calculated 20% width and the Strehl ratio I_s vs the mismatch angle: a, width in the meriidonal plane for the x direction; b, the same for the y direction; c, width in the sagittal plane for the x direction; d, Strehl ratio in the meridional plane; e, Strehl ratio in the sagittal plane. The dots illustrate the measured data for a.

A more radical change can be seen in Fig. 7 for $\delta_\kappa = 2 \times 10^{-4}$ and 10^{-3} rad. (Note the change of the scale.)

We summarize the results of calculations in Fig. 8, where the width of the 20% isophotes is illustrated for the meridional plane in the x and y directions. The sagittal plane is shifted by $\xi = 2\alpha x_0$ from the Gaussian plane; the 20% width in the x direction is also shown in this plane. Definitive oscillations of the width—superimposed on a constant rise—can be found.

As has been mentioned the mismatch causes widening of the wings of the distribution, i.e., an amount of the energy is spread out. Figure 8 shows that the tolerance condition $\delta_\kappa < 10^{-5}$ rad is inevitable, because the Strehl ratio falls very rapidly, which may lead to underexposed holographic copies.

For mismatch angles of 0, 5×10^{-5}, and 2×10^{-4} rad the intensity distribution was scanned by a microphо-

tometer consisting of an objective with a N.A. of 0.85 and a projective, the total magnification was between 30 and 80 for individual scans (it was measured after each readjustment). The light was projected on a pinhole of 12.5-μm diameter and detected by a photomultiplier. The microscope was micropositioned by an alignment of five degrees of freedom and the picture with minimum stray light was set visually.

The measured spatial intensity distribution is illustrated in Figs. 6 and 7, the 20% width in Fig. 8. It is noteworthy that the relative deviation from the calculated width increases as the intensity parameter of the isophotes becomes smaller. The sloping part of the distribution seems to be caused by the deviation of the hologram glass substrate from ideal flatness. This supposition was supported by experience when the transfer of line shaped objects was studied and an unambiguous relation between the slowly varying thickness and the stray light was found.

IV. Conclusions

Holograms, in principle, offer the possibility of high resolution imaging for an extended object field. If 1:1 imaging is required—as is the case for photolithography—one needs to use a plane reference beam and a plane reconstructing beam, opposite in direction, to obtain a real image in place of the object. This setup corresponds to four-wave mixing.

However, the holographic system should be adjusted with regard to the direction of the auxiliary rays using the highest precision allowed by the aperture used. It was shown in a simple way that, if the mismatch angles between the auxiliary rays are >1 mrad, remarkable geometrical aberrations occur when a holographic recording system with reasonable parameters is used. For smaller mismatch the aberrations remain, but they are folded with wave diffraction; this factor was taken into account by the only possible way for large apertures, i.e., numerical computation. The calculations and measurements are in agreement within the defect of the hologram plate.

It should be stressed that simultaneously with the widening of the pattern the more rapid falling of the Strehl ratio can cause major problems in application.

Observed effects and calculations are applicable for the case of real-time holography, i.e., four-wave mixing. In this case any irregularities in the phase front of the pumping waves are enlarged by the nonlinear response of the mixing medium, or the medium may have defects itself, consequently appreciable spread of the light may diminish the quality of the real-time image.

References

1. W. H. Carter and A. A. Dougal, "Field Range and Resolution in Holography," J. Opt. Soc. Am. **56,** 1754 (1966).
2. D. H. R. Vilkomerson and D. Bostwick, "Some Effects of Emulsion Shrinkage on a Hologram's Image Space," Appl. Opt. **6,** 1270 (1967).
3. E. B. Champagne, "Nonparaxial Imaging, Magnification and Aberration Properties in Holography," J. Opt. Soc. Am. **57,** 51 (1967).
4. E. B. Champagne and N. G. Massey, "Resolution in Holography," Appl. Opt. **8,** 1879 (1969).
5. J. Nowak and M. Zajac, "Numerical Investigations of Holographic Imaging Quality," Opt. Appl. **15,** 239 (1985).
6. K. Peng and H. J. Frankena, "Nonparaxial Theory of Curved Holograms," Appl. Opt. **25,** 1319 (1986).
7. E. L. O'Neil, *Introduction to Statistical Optics* (Addison-Wesley, Reading, MA, 1963), p. 50.
8. Formulas describing the geometric aberrations can be obtained from the works[3–7] already cited. In these papers the auxiliary waves are spherical and a transition is to be performed for the telecentric case. However, we preferred a straightforward calculation to show the presence of aberrations—in the most simple case—by a direct way and a short way. The method of deduction of the formulas follows that given in Ref. 3.
9. M. Born and E. Wolf, *Principles of Optics* (Pergamon, London, 1959), Chap. 9.
10. G. Kiss, "Effect of Optical System Imperfections on Probability of Holographic Memory Failures," Kvantovaya Elektron. **11,** 1947 (1984), in Russian.

Meetings *continued from page 1284*

1988
June

4–8 Medical China '88, Hangzhou *G. Kallman, Kallman Assocs., 5 Maple Court, Ridgewood, NJ 07450*

5–9 1988 Computer Vision & Pattern Recognition Mtg., Ann Arbor *IEEE, E. 42nd St., New York, NY 10017*

6–8 Laser Technologies in Industry Int. Conf., Porto *Sec.: Laser Tech. in Industry, Laboratorio de Fisica, Faculdada de Ciencias, Universidade do Porto, 4000 Porto, Portugal*

6–10 Infrared Technology & Applications course, London *Sira Ltd., South Hill, Chislehurst, Kent BR7 5EH, U.K.*

6–10 Electro-Optical System Analysis course, El Segundo *UCLA Ext., P.O. Box 24901, Los Angeles, CA 90024*

6–10 Human Factors in Displays & Controls course, El Segundo *UCLA Ext., P.O. Box 24901, Los Angeles, CA 90024*

7–9 Optical Storage for Large Systems Mtg., New York *TOC, P.O. Box 14817, San Francisco, CA 94114*

7–10 Photographic Instrumentation Techniques course, Rochester *RIT/T&E Sem. Ctr., 1 Lomb Memorial Dr., Rochester, NY 14623*

12–15 Int. Conf. on Electronic Materials in Japan, Tokyo *T. Kamiya, Dept. Electronics Engineering, U. Tokyo, 7-3-1- Hongo Bunkyo-kum Tokyo 113, Japan*

14–19 China Optoelectronics Laser '88, Beijing *Cahners Expo. Group, P.O. Box 70007, Wash., DC 20088*

15–16 Fiber Optics in Plain English Sem., Atlanta *Trellis Communications Corp., 5 Manor Pkwy., Salem, NH 03079*

continued on page 1312